J. Fluid Mech. (2025), *vol.* 1015, A56, doi:10.1017/jfm.2025.10383

JFM PAPERS

Vortices, shocks and non-linear acoustic waves: the ingredients for resonance in impinging compressible jets

Daniel Michael Edgington-Mitchell[1], **Joel Luke Weightman**[1], **Soudeh Mazharmanesh**[1] and **Petronio Nogueira**[1]

[1]Shock Lab, Monash University Department of Mechanical and Aerospace Engineering, Clayton, Australia

Corresponding author: Daniel Michael Edgington-Mitchell, daniel.m.mitchell@gmail.com

(Received 23 October 2024; revised 7 April 2025; accepted 10 May 2025)

Compressible jets impinging on a perpendicular surface can produce high-intensity, discrete-frequency tones. The character of these tones is a function of nozzle shape, jet Mach number, impingement-plate geometry, and the distance between nozzle and plate. Though it has long been recognised that these tones are associated with a resonance cycle, the exact mechanism by which they are generated has remained a topic of some debate. In this work, we present evidence for a number of distinct tone-generation mechanisms, reconciling some of the different findings of prior authors. We demonstrate that the upstream-propagating waves that close resonance can be confined within the jet, or external to it. These waves can be either weak and relatively linear, or strong and nonlinear from their inception. The waves can undergo coalescence or merging, and in some configurations, pairs of waves rather than singletons appear. We discuss both historical and new evidence for multiple distinct processes by which upstream-propagating waves are produced: direct vortex sound, shock leakage, wall-jet-boundary fluctuations, and wall-jet shocklets. We link these various mechanisms to the disparate collection of upstream-propagating waves observed in the data. We also demonstrate that multiple mechanisms can be provoked by a single vortex, providing an explanation as to why sometimes pairs of waves or merging waves are observed. Through this body of work, we demonstrate that rather than being in opposition, the various pieces of past research on this topic were simply identifying different mechanisms that can support resonance.

Key words: jet noise, supersonic flow, shock waves

1. Introduction

When a jet impinges upon a surface, the interaction between the jet and the surface produces significantly more sound than the jet alone. While some of this sound is broadband, at certain conditions, there is also a significant tonal component to the noise (Marsh 1961; Powell 1988). This tonal behaviour is exhibited by both subsonic (Nosseir & Ho 1982) and supersonic (Henderson 2002) jet flows, and is well recognised to be the result of a resonant feedback loop (Edgington-Mitchell 2019). This resonance process can be well described using a classical long-range resonance model, as proposed by Powell (1988), consisting of four discrete processes: the downstream propagation of energy, a reflection mechanism at the plate surface that redirects some of this energy upstream, the upstream propagation of energy, and a reflection mechanism at the nozzle.

The downstream propagation of energy is the best understood of these processes; the introduction of a solid surface downstream does not qualitatively change the fundamental mechanisms compared to an isolated or 'free' jet. In both cases, energy is extracted from the mean flow via the well-known Kelvin–Helmholtz (KH) convective instability. In free jets, the growth, saturation and eventual decay of the structure that finds its inception in the KH instability is typically referred to as a wavepacket, due to its spatial-amplitude envelope (Jordan & Colonius 2013). For many impinging-jet configurations, the plate is located before the peak of this amplitude envelope, meaning that the overall behaviour of the downstream process is only qualitatively similar to the 'wavepacket' behaviour seen in free jets. Nonetheless, the same fundamental shear-layer instability mechanism is at work in both free and impinging jets

The reflection mechanism at the nozzle lip is also relatively well understood at a conceptual level, being essentially a shear-layer receptivity process. This process is difficult to observe directly, due to the extremely small time and length scales, but high-magnification schlieren visualisations demonstrate that (at least for the nonlinear waves that occur for some impinging-jet configurations) a strong perturbation of the thin shear layer rapidly grows via the KH instability to produce the downstream-propagating wave (Mitchell, Honnery & Soria 2012). This process has been investigated in more detail numerically (Karami *et al.* 2020*a*,*b*), where it was demonstrated that the initial response of the shear layer to an almost-impulsive forcing is relatively broadband in the high-frequency range, but this initial broadband perturbation evolves into a single large vortex within the first nozzle diameter.

The upstream process, one of the two foci of this paper, is somewhat more contentious. Historically, in both free and impinging jets, this upstream wave was assumed to be a freely propagating acoustic wave. Such an assumption is the basis for the classical screech (Powell 1953) and impingement (Powell 1988) models of Powell. In the seminal work of Tam & Hu (1989), it was demonstrated that the linearised Navier–Stokes equations predicted that an acoustic-like but discrete mode could also be supported by the flow. This wave, which would later come to be referred to as the guided jet mode, was shown by Tam & Ahuja (1990) to provide a more rigorous prediction of resonance in high-subsonic and low-supersonic Mach number jets than models considering a classical freestream acoustic wave. The literature is now replete with examples of this guided jet mode underpinning resonance, in the potential core of free subsonic jets (Towne *et al.* 2017), in jets grazing against flaps (Jordan *et al.* 2018), and in screeching jets (Gojon, Bogey & Mihaescu 2018; Edgington-Mitchell *et al.* 2018, 2022; Nogueira *et al.* 2022).

The nature of this discrete mode was recently revealed in Nogueira *et al.* (2024). In this work, the authors showed that the guided jet mode is in fact how the linearised Navier–Stokes equations represent an acoustic wave generated within the jet, that is undergoing reflection and transmission at the shear layer. In the region of the flow where a sound source is bounded by the jet shear layer, waves produced by this source will have the properties of a guided wave: a phase velocity slightly below the ambient speed of sound, and a finite band of frequencies for which the wave can be supported. Thus in Nogueira *et al.* (2024), the role of this guided jet mode in resonance was revealed: if the downstream reflection mechanism is located inside the core of the jet, then resonance can occur only if the guided mode is supported by the flow, i.e. if reflection and transmission can produce a net energy flux in the upstream direction. In the case of subsonic or screeching free jets, this explains why resonance is observed only when the flow supports the guided jet mode; for these flows, the sound sources themselves are located inside the jet. In impinging jets, the situation is somewhat more complicated. Since the first demonstration by Tam & Ahuja (1990), there have been multiple follow-up studies, primarily in the form of high-fidelity numerical simulations, that suggest that the guided jet mode must be supported for impingement tones to be observed. These studies include jets ranging from the subsonic (Varé & Bogey 2022*a*, 2023) to the supersonic (Gojon & Bogey 2017; Bogey & Gojon 2017), and the evidence presented therein is strong, with the radial structure of observed upstream-propagating waves matching the eigenfunctions predicted by linear theory, and the observed frequencies matching the predictions of models based on the existence of the guided jet mode. In contrast to this, the work of Henderson *et al.* (2005) and Weightman *et al.* (2017*b*, 2019) on impinging underexpanded jets clearly reveals a freestream nonlinear shock-like wave closing the resonance loop, a wave that can be observed to originate from outside the jet shear layer. In the most extensive experimental parametric study of impinging jets, Jaunet *et al.* (2019) demonstrated that models based on the guided jet mode had mixed success across a wide range of operating conditions, correctly predicting some tones but missing others. Consistent with these experimental data, an extensive numerical survey by Ferreira *et al.* (2023) likewise showed excellent agreement for subsonic jets, and more mixed results for supersonic jets. Why this inconsistency? From the results presented in Nogueira *et al.* (2024), the guided jet mode is relevant only when the sound is generated from within the region of the jet bounded by the shear layer. Thus to determine when the frequency bands of the guided jet mode will govern resonance, we must consider the mechanism by which upstream-propagating waves are generated at the surface. At this juncture, it is also perhaps helpful to consider that many of the upstream-propagating waves that we will consider in this work are of sufficient amplitude that they are poorly described by linearised forms of the governing equations (Hamilton & Blackstock 2024). In jet aeroacoustics, there are several potential sources for nonlinear waves: waves that steepen during propagation (Gee *et al.* 2008; Reichman *et al.* 2022), waves produced due to the coalescence of multiple waves in the jet near field (Fiévet *et al.* 2016; Willis *et al.* 2023), and waves that are nonlinear or even shock-like from their inception (Young *et al.* 2015; Pineau & Bogey 2019). In this paper, given that the largest distance between source and nozzle that we consider is less than ten nozzle diameters, and our nozzles are very small, nonlinearity due to propagation will be insignificant Baars *et al.* (2014). Thus we are principally concerned with the other sources of nonlinearity, coalescence and nonlinear source mechanisms.

The final process to consider then is the generation process: how are the upstream-propagating waves generated, and where in the flow are they generated? Figure 1 presents a schematic overview of an impinging supersonic jet, with an exemplar schlieren image. In this schematic, we represent the three mechanisms of upstream-wave production that have been demonstrated in the literature: (*a*) wall-jet-boundary displacement (Henderson *et al.* 2005), (*b*) direct vortex sound (Varé & Bogey 2022*a*) and (*c*) the wall-jet shocklet (Weightman *et al.* 2017*b*). In the case of underexpanded impinging jets, both annular and continuous stand-off shocks have been observed (Henderson 2002), and these two

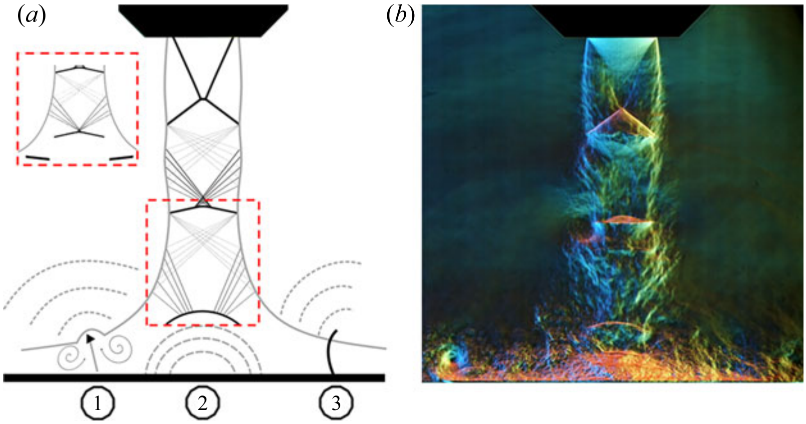

Figure 1. (*a*) Schematic of supersonic impinging jet flow, with (*b*) accompanying colour schlieren visualisation. Shown in the schematic are the three existing proposed modes of sound generation in compressible jet impingement: (1) the wall-jet fluctuation mechanism of Henderson, Bridges & Wernet (2005); (2) the direct interaction with the plate as quantified in Varé & Bogey (2022*a*); and (3) the wall-jet shocklet mechanism of Weightman *et al.* (2017*b*). The inset presents an alternative shock configuration that arises at some conditions, with an annular plate shock structure.

configurations are also presented. Why are there multiple mechanisms? If for some configurations resonance can occur only when the mean flow is capable of supporting the reflection and transmission processes that characterise the guided jet wave, then in these cases the generation of upstream waves must take place inside the jet. Conversely, in cases where the observed resonance frequency is incompatible with the support of the guided jet mode, such as some cases observed in Jaunet *et al.* (2019) and Ferreira *et al.* (2023), the upstream wave must be generated outside the core of the jet. In the first proposed example of the guided waves closing the resonance loop (Tam & Ahuja 1990), no specific mechanism of upstream-wave generation was proposed, other than stating that the generation occurs when the KH waves reach the impingement surface. In the Fourier-decomposed pressure fields presented in Gojon, Bogey & Marsden (2016) and Bogey & Gojon (2017), the peak pressure fluctuations at the resonance frequency occur at the centreline of the jet, just above the impingement surface. If this fluctuation peak can be considered the effective source, then the evidence produced by Bogey & Gojon (2017), that the impingement tones correspond to frequencies where the guided jet mode is supported by the flow, is consistent with what we now know about this wave. Why is the effective sound source at the centreline? In an attempt to specify a particular mechanism associated with the generation of upstream-propagating acoustic waves, Varé & Bogey (2022*a*) used Curle's analogy to calculate the one component of the sound produced by an impinging jet. In their implementation of the analogy, they considered only the sound field produced by the pressure exerted on the surface by the flow. Considering only this flow–surface interaction, they were able to achieve an excellent qualitative match between the pressure field observed in the large-eddy simulations and the predictions from Curle's analogy. The work of Varé & Bogey (2022*a*) is, to the best of the authors' knowledge, the first time an attempt has been made to rigorously link a specific sound-producing mechanism and the resultant acoustic field. These results and what they imply for our understanding of impinging-jet resonance will be discussed further in § 4.

In prior research where the guided jet mode was taken as the upstream component of resonance, with the exception of the aforementioned research by Varé & Bogey (2022*a*), discussion has typically focused on the nature of the upstream-propagating wave, rather

https://doi.org/10.1017/jfm.2025.10383 Published online by Cambridge University Press

than the mechanism by which it is generated. Conversely, works that consider a freestream wave often describe more specific mechanisms of upstream-wave generation, and thus more specific source locations. Powell (1988) suggested that for supersonic jets with strong shocks, the large-scale vortical structures would generate oscillations of the stand-off shock. The motion of the stand-off shock would then produce downstream-propagating pressure waves that reflect from the impingement surface before escaping through the periphery of the jet to propagate upstream. An alternative theory was later proposed, supported with more sophisticated measurement techniques in the work of Henderson *et al.* (2005), suggesting that the arrival of the vortices associated with the KH wave produced a large fluctuation in the wall jet; the movement of the wall-jet boundary was thought to act like a membrane, producing an acoustic wave via the displacement of a surface. A key component of this work was identifying that the source of the acoustic wave was located far from the jet-impingement point, at $r/D \approx 1.3D$. More recently, time-resolved visualisation of an impinging jet identified a transient shock in the wall-jet at a similar location ($r/D \approx 1.3D$); the motion of this shocklet was directly observed to produce an upstream-propagating acoustic wave (Weightman *et al.* 2017*b*). A consideration of the time scales associated with the formation of this shocklet and the resultant transmission of an upstream wave was sufficient to explain the ‘phase lag’ term in Powell’s original resonance formulation. In another more recent study (Weightman *et al.* 2019), a section of the stand-off shock was observed to detach and become upstream propagative, in a manner reminiscent of the shock-leakage process in a screeching jet (Edgington-Mitchell *et al.* 2021).

This paper, an extension of preliminary work documented in Edgington-Mitchell, Weightman & Nogueira (2024), thus sets out to resolve this apparent discrepancy in sound-generation mechanism in a number of reported studies. Though not the focus of this paper, when the impingement plate is located sufficiently far from the nozzle, screech tones can coexist with impingement tones, as discussed in Sinibaldi *et al.* (2013) and Liu *et al.* (2021). We will consider the three sound-generation mechanisms shown in figure 1, as well as discussing some others. In so doing, we will attempt to address several open questions. Is there actually a disagreement in the literature, or are there simply different mechanisms active at different Mach numbers or impingement distances? Is the sound-production mechanism dependent on Mach number? What about the source location? To answer these questions, we will provide details of the experimental configuration in § 2, before classifying the various forms of upstream wave in § 3, and the mechanisms by which these waves are generated in § 4.

2. Experimental methodology

Our study of impinging-jet resonance spans a broad range of nozzle pressures, stand-off distances, and nozzle and impingement-surface geometries. The four nozzle geometries considered are presented in table 1: two axisymmetric and two rectangular nozzles of aspect ratio $AR = 2$, with each shape having one purely converging and one method of characteristics (MOC) converging–diverging variant. Both axisymmetric nozzles have been used extensively in the study of impinging-jet resonance previously (Weightman *et al.* 2017*a*, 2019), while the sharp-throated rectangular nozzle has formed the basis for numerous studies on flow control in single and dual jets (Webb *et al.* 2023; Samimy *et al.* 2023, 2024). The variation in effective nozzle diameter shown in table 1 means that the Reynolds number ($Re = U_j D_J/\mu$) differs by a factor of approximately two between the smallest and largest nozzles at the same nozzle-pressure ratio, but given that the lowest Reynolds number considered is still $O(10^5)$, the observed phenomena

Nozzle schematic	Exit geometry	Internal geometry	NPR_D	D_e	t/D_e
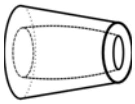	Axisymmetric	Converging	1.9	15 mm	0.3
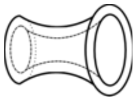	Axisymmetric	Converging–diverging (MOC)	4.0	11 mm	0.6
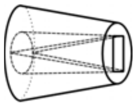	Rectangular	Converging	1.9	13.6 mm	0.6
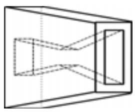	Rectangular	Converging–diverging (sharp-throated)	3.7	8.7 mm	0.5

Table 1. Nozzle geometries used in this study: NPR_D indicates design pressure ratio, D_e is equivalent circular diameter at the nozzle exit, and t/D_e is average non-dimensional lip thickness.

are assumed to be insensitive to this variation. McLaughlin, Morrison & Troutt (1977) showed minimal changes in the acoustic field of a supersonic jet as Reynolds number was varied from $O(10^3)$ to $O(10^5)$, and Ozawa *et al.* (2020) demonstrated that unless a flow was transitional, the acoustic field showed little sensitivity to Reynolds number. All four nozzles have relatively thick lips; resonance in jets is highly sensitive to lip thickness (Weightman *et al.* 2019). Note also that the rectangular nozzles have non-uniform lip thicknesses; the purely converging nozzle has a circular lip, whereas the sharp-throated nozzle has a rectangular lip whose thickness is proportional to each axis, rather than the equivalent diameter. All measurements were conducted in the Gas-Jet Facility at Monash University, which supplies unheated dry air to the aforementioned nozzles through a flow-conditioned plenum; detailed discussions of the facility are available in the aforementioned papers, and repetition here is omitted for brevity.

Several geometries for the impingement surface were also considered. The canonical flat-plate impingement configuration, which is the most studied and application-relevant set-up, can render observation of some key features difficult due to the path-integrated nature of schlieren. Previous research has demonstrated that the flapping axis of an axisymmetric jet can be locked to a particular orientation through the use of a cylindrical impingement surface (Mason-Smith *et al.* 2015); a cylindrical surface with radius 37.5 mm is used for most of the visualisations presented herein. Large parametric sweeps were also performed with the simple flat-plate geometry, though only select results are presented here. Direct visualisation of the wall-jet shocklet has previously been easiest with a hemispherical impingement surface, as the degree of path integration through the wall jet is minimised. In this work, a hemisphere with the same radius 37.5 mm was used to aid in visualisation of certain cases where the dynamics are particularly complex. At given jet-operating condition and impingement-plate distance, the resonance process will certainly be quantitatively different for a flat plate than a curved surface. However, all the

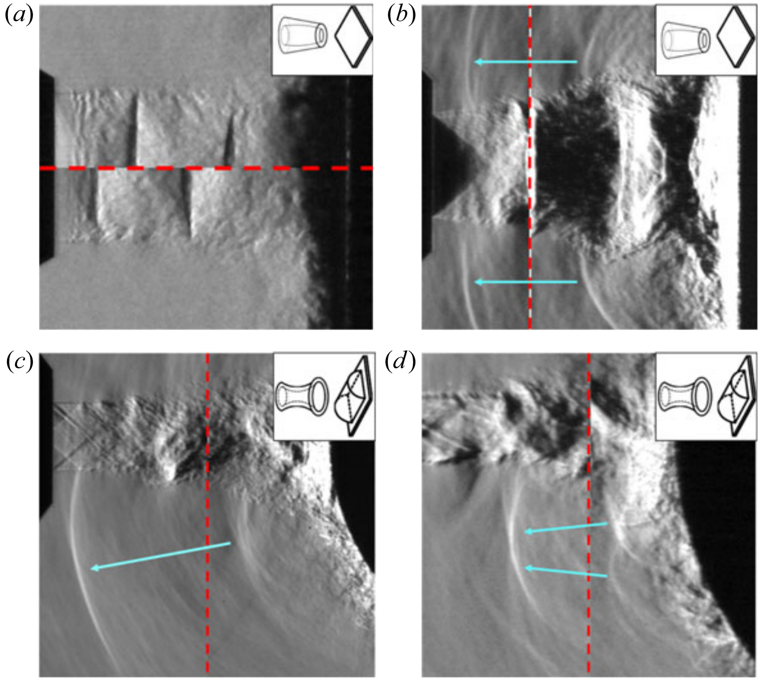

Figure 2. Four qualitatively different upstream-propagating waves observed in compressible jet impingement: (*a*) nonlinear duct-like waves; (*b*) nonlinear freestream acoustic waves; (*c*) steepening freestream acoustic waves; (*d*) merging nonlinear freestream waves. The inset in each image indicates the nozzle and impingement geometry used to produce that image. The dashed red line separates the two snapshots that were used to produce the composite images.

phenomena that will be shown in this paper for curved surfaces can also be observed for flat plates, simply with less clarity.

Both shadowgraph and schlieren visualisation were used in this study, producing images whose intensity is proportional to $\nabla^2\rho$ or $\partial\rho/\partial x$, respectively. A Z-type Toepler schlieren system was used for both imaging modalities, with the knife-edge removed and the image slightly defocused in the case of shadowgraph. Illumination was provided via a pulsed LED (Willert, Mitchell & Soria 2012) with pulse width 500 ns, and images were recorded on a Photron Fastcam SA-Z 2100k camera with varying frame rate (50–200 kfps) and resolution.

3. Upstream-propagating waves

We begin our discussion of the ways the upstream propagation of energy can occur in these jets by gathering visualisations of all the various families of waves that this flow can support. Figure 2 presents exemplar schlieren images of some of the waves that we will discuss in this paper; each of these images is a composite of two schlieren images with a short time delay $O(10^{-5}\ \mathrm{s})$ between them, with the dashed red line indicating the point of division. In the subsonic jet shown in figure 2(*a*), the upstream-propagating wave is nonlinear and duct-like. In contrast, figure 2(*b*) presents waves propagating in the freestream rather than inside the flow; the jet in this case, and the following images, is supersonic. Figure 2(*c*) shows an initially diffuse collection of waves coalescing into a single strongly nonlinear wave, while figure 2(*d*) instead reveals the merging of two strong waves into a single stronger wave. In this section, we will consider these four examples, as well as several others, in more detail.

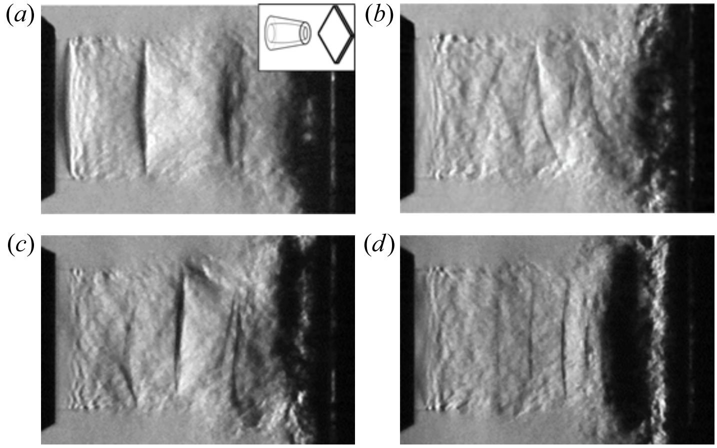

Figure 3. Nonlinear duct-like modes observed in high-subsonic jet impingement for $z/D = 2$: (*a*) $m = 0$ mode at $M = 0.86$; (*b*) $m = 1$ mode at $M = 0.88$; (*c*) $m = 1$ mode at $M = 0.89$; (*d*) $m = 0$ mode at $M = 0.90$. The Reynolds number spans $Re = [3.0 \times 10^5, 3.7 \times 10^5]$. The directory including exemplar image sequences for this figure and the accompanying Jupyter notebook can be accessed at https://www.cambridge.org/S0022112025103832/JFM-Notebooks/files/Figure3/Figure3.ipynb.

3.1. *Duct-like upstream-propagating waves and the guided jet mode*

The first upstream-propagation mechanisms that we consider are the duct-like modes presented in figure 3. These are the same waves predicted theoretically by Tam & Hu (1989), suggested to govern subsonic jet resonance in Tam & Ahuja (1990), and recently observed experimentally for the first time in Li *et al.* (2024). The present data, however, provide some surprising detail regarding the nature of these waves. In still frames, the upstream-propagating waves look distinctly like the stationary shock waves formed in an underexpanded jet; however, as demonstrated in figure 2(*a*), these waves are actually propagating upstream. Though these waves are well predicted by linear models, here their amplitude is sufficiently strong that their interaction with the mean flow is nonlinear, more closely resembling a train of upstream-propagating shock waves rather than acoustic waves. While the waves associated with the $m = 0$ azimuthal mode evident in figures 3(*a*) and 3(*d*) bear a resemblance to the stationary shock cells for an underexpanded jet, figure 3(*b*,*c*) reveal that waves associated with an $m = 1$ resonance trace a helical pattern through the core of the jet that has no analogue in steady supersonic flow.

As discussed in § 1, predictive models for resonance that assume that the upstream-propagating wave is the duct-like mode (or the equivalent guided jet mode) of figure 3 perform very well for subsonic jets and some ideally expanded (Varé & Bogey 2023) and underexpanded (Ferreira *et al.* 2023) supersonic jets. A visual inspection of the Fourier-decomposed pressure fields presented in Bogey & Gojon (2017) and Gojon & Bogey (2017) illustrate why: the pressure fields inside and outside the jet are almost uncorrelated for some underexpanded-jet cases, which indicates that the upstream-propagating wave cannot be the guided jet mode. In other cases, a waveform that is contiguous across the shear layer is evident, consistent with the structure of the guided jet mode. The majority of ideally expanded jet cases also exhibit this contiguous waveform. For the cases where the phase of the wave is uncorrelated across the shear layer, a different form of wave must be involved in the resonance. In the next subsection, we instead consider an upstream-propagating wave that exists entirely in the freestream.

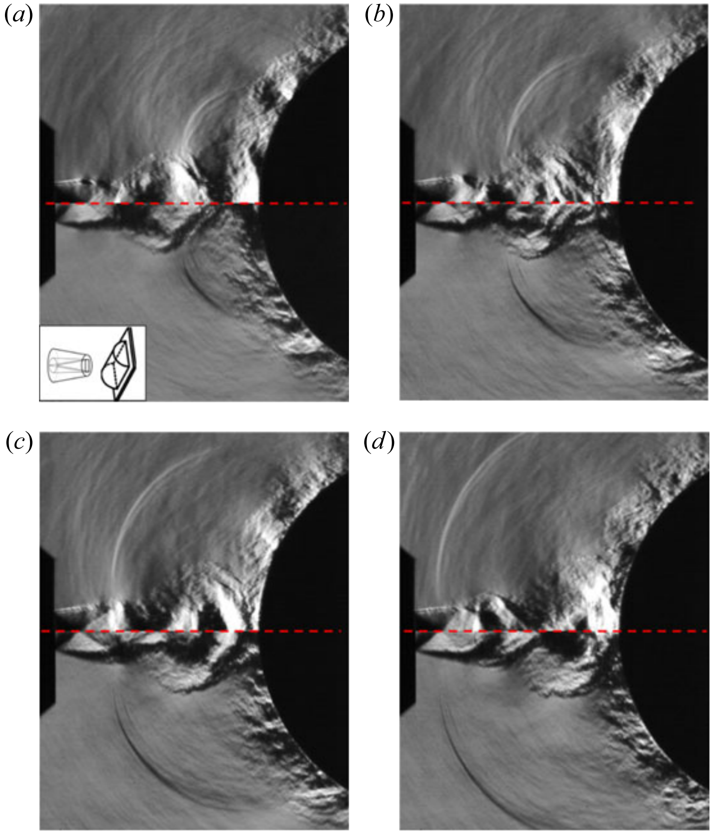

Figure 4. A nonlinear acoustic wave propagating through the freestream exterior to the jet. (*a*–*d*) A time series with 200 μs between each frame; here, $NPR = 3.0$, $z/D_e = 3$, $Re = 6.5 \times 10^5$. Visualisations are a composite of $\partial\rho/\partial x$ (upper) and $\partial\rho/\partial y$ (lower); the two visualisations were taken separately and manually phase matched. The directory including exemplar image sequences for this figure and the accompanying Jupyter notebook can be accessed at https://www.cambridge.org/S0022112025103832/JFM-Notebooks/files/Figure4/Figure4.ipynb.

3.2. *Freestream upstream-propagating waves*

The second form of upstream-propagating wave that we consider is a nonlinear wave travelling in the freestream, an example of which is shown in figure 4. These images, which are *a posteriori* reconstructions based on images of both the $\partial\rho/\partial x$ and $\partial\rho/\partial y$ gradients, were obtained from the visualisation of a jet from a converging rectangular nozzle at $NPR = 3.0$, impinging on a cylindrical surface at height $z/D_e = 3.0$. The sensitivity of the schlieren technique to the direction of wave propagation is highlighted here; sections of the wave are missing in each gradient-field image. The strong nonlinearity of this wave is evident in the sharpness of the wavefront visible in the schlieren data, indicative of something more resembling an inverse-sawtooth rather than sinusoidal wave. To more clearly define the shock-like nature of these waves, we reconsider particle image velocimetry (PIV) data presented in Weightman *et al.* (2016). These data concern a jet from the converging axisymmetric nozzle operating at pressure ratio $NPR = (p_0/p_\infty)$ and impinging on the cylindrical surface at $z/D = 3.5$. A contour of instantaneous streamwise velocity fluctuation is presented in figure 5, along with two streamwise velocity profiles extracted by averaging across 20 vectors in the vertical direction. Sharp wavefronts are visible in the acoustic field of the jet on both sides, corresponding to the

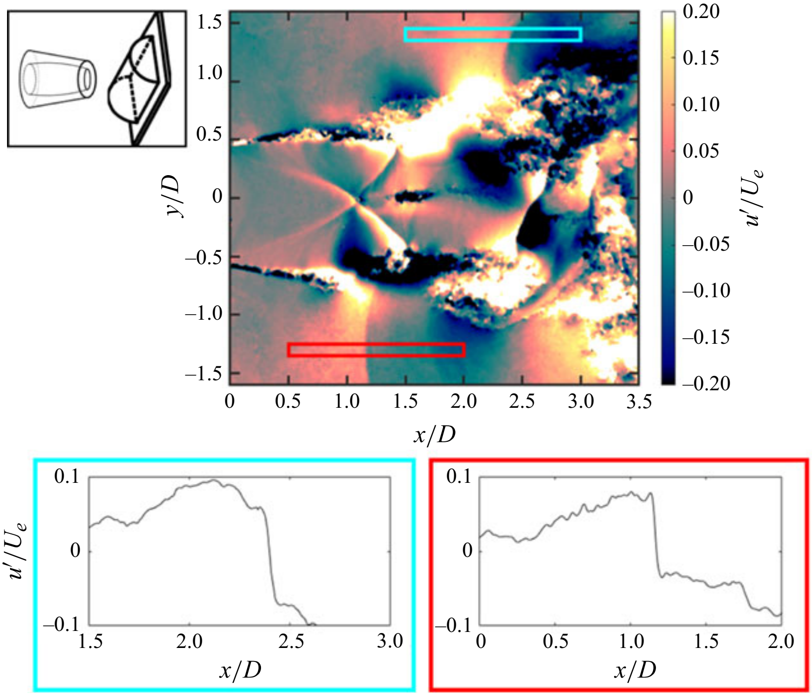

Figure 5. Instantaneous fluctuating velocity field obtained from PIV data in Weightman *et al.* (2016). Profiles are streamwise velocity, averaged over 20 vectors in the radial direction, corresponding to coloured rectangles superimposed on the contour map.

upstream-propagating wave that forms part of the resonance loop. Considering that the streamwise velocity change across the waves is $\Delta u \approx 40\,\mathrm{m\,s^{-1}}$, the Rankine–Hugoniot relations indicate that the wave is in fact a shock with Mach number $M_s \approx 1.07$, which would correspond to an effective sound pressure level $SPL \approx 175\,\mathrm{d}B$. The regions over which the velocity is calculated are not exactly normal to the wave, so the actual Mach number may be slightly higher. Though the curves in figure 5 do not seem to exhibit a step change in velocity, this is due to the well-known particle lag behind the shock wave (Melling 1997); considering the PIV and schlieren together, it is clear that this wave is shock-like.

These upstream-propagating nonlinear freestream waves are visible in the data at a wide range of operating conditions. Figure 6 presents an example from the converging–diverging axisymmetric nozzle, operating close to its design point $NPR = 4.0$, and impinging on the cylindrical surface at distance $z/D = 4.5$. Figure 6(*a*) represents an initial snapshot in time, where a wave that has just reached the nozzle plane is visible, as well as a newly created wave at $x/D \approx 3.5$; it is the latter wave that we will track in this image. Figure 6(*c*) represents the penultimate wave position considered in this figure, while figure 6(*b*) presents three snapshots of the wave as it propagates upstream. Figure 6(*d*) presents streamwise plots of light intensity, averaged across 40 px in the vertical direction, plotted as a function of distance from the nozzle. The shape of the wavefront, at least as captured in the schlieren visualisation, changes minimally during its upstream propagation; the peak amplitudes are similar, as are the half-widths.

A careful examination of figure 6(*c*) reveals the presence of a different phenomenon: a new diffuse wavefront at $x/D \approx 4.0$, seemingly replacing the sharp nonlinear wave from figure 6(*a*) in the next period of the resonance cycle. Figure 7 presents a clearer

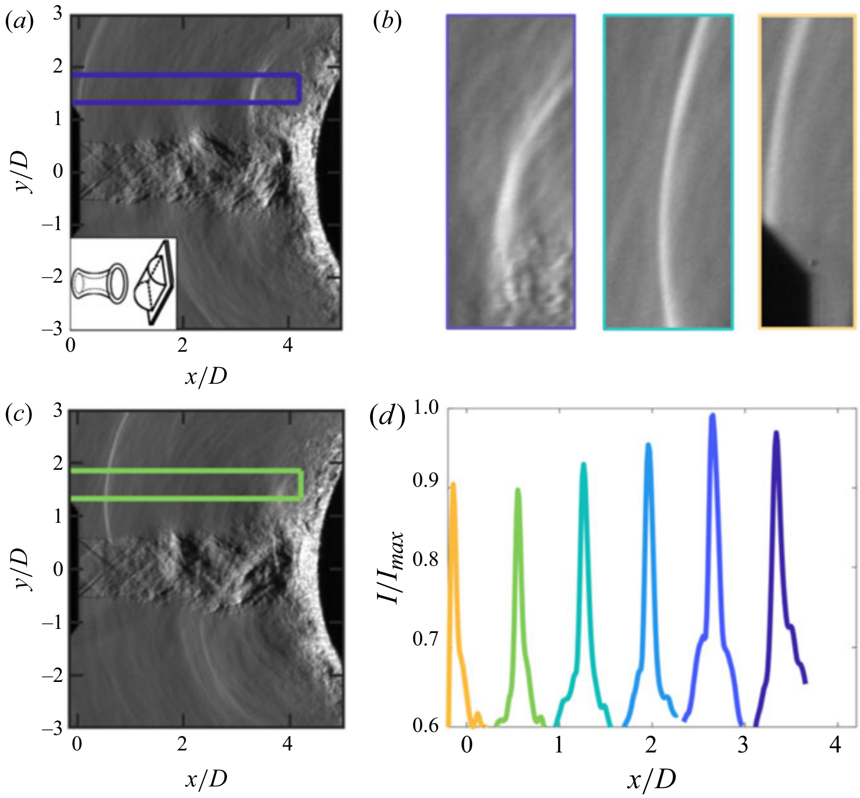

Figure 6. Upstream-propagating wave that is nonlinear from its inception, with $NPR = 4.0$, $z/D = 4.5$, $Re = 6.5 \times 10^5$. (*a,c*) $\partial\rho/\partial x$ schlieren visualisations of the first and last instants where the exemplar upstream-propagating wave is visible. (*b*) Schlieren visualisations of the upstream-propagating wave in the Lagrangian frame of reference. (d) Image intensity profiles across the upstream-propagating wave as a function of axial position. The directory including exemplar image sequences for this figure and the accompanying Jupyter notebook can be accessed at https://www.cambridge.org/S0022112025103832/JFM-Notebooks/files/Figure6_7.

exemplar of this less-shock-like wave; the initial wavefront at $x/D = 3.5$ in figure 7(*a*), presented in close-up in figure 7(*b*), appears to represent a diffuse collection of waves, rather than a single nonlinear wave. Tracking this collection of waves as it moves upstream reveals a relatively rapid coalescence into a single sharp wavefront, with a narrow peak of high amplitude appearing by $x/D \approx 2$. During this coalescence, the half-width of the intensity peak shrinks dramatically, along with a concomitant increase in the peak amplitude. Strong acoustic waves undergoing nonlinear steepening during propagation is a well-known phenomenon (Gee *et al.* 2008; Baars *et al.* 2014), though it is difficult to ascertain from these data whether we are observing a classical nonlinear steepening, the coalescence of waves from distributed sources, or most likely a combination of both. It is perhaps worth emphasising at this point that figures 6 and 7 are obtained from the same sequence of images, and as is clear from the sequence in figure 6, switching between sharp and diffuse waveforms can occur over a single period of the resonance cycle. No clear link between the amplitude or shape of the downstream-propagating KH wavepacket and the sharpness of the upstream-propagating wave could be educed from the data.

If we continue with our consideration of an axisymmetric jet impinging on a cylinder, which has so far been able to produce both shock-like waves and coalescing waves, then a

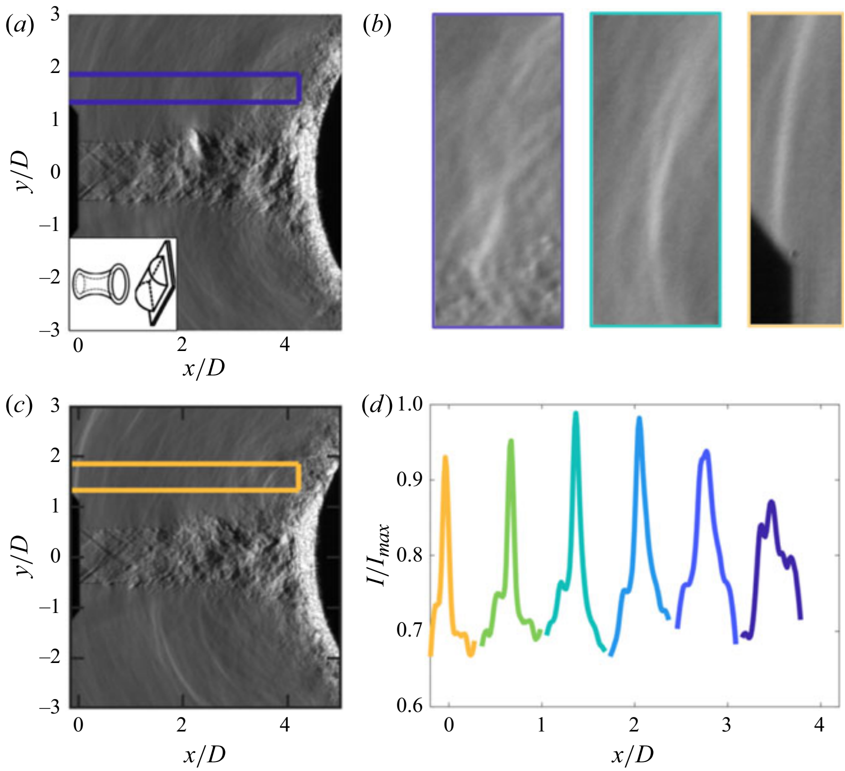

Figure 7. Acoustic waves undergoing coalescence to form a single nonlinear wave, with $NPR = 4.0$, $z/D = 4.5$, $Re = 6.5 \times 10^5$. (*a*,*c*) $\partial\rho/\partial x$ schlieren visualisations of the first and last instants where the exemplar upstream-propagating wave is visible. (*b*) Schlieren visualisations of the upstream-propagating wave in the Lagrangian frame. (*d*) Image intensity profiles across the upstream-propagating wave as a function of axial position. The directory including exemplar image sequences for this figure and the accompanying Jupyter notebook can be accessed at https://www.cambridge.org/S0022112025103832/JFM-Notebooks/files/Figure6_7.

further increase in nozzle pressure ratio to $NPR = 4.8$ will introduce yet another member of the upstream-propagating-wave family: a merging of two initially nonlinear waves, as depicted in figure 8. Here, we have two shock-like waves that appear to have originated from different sources in the impingement region or wall jet, that merge together into a single complex waveform. As described in detail in Willis *et al.* (2023), the merging of two nonlinear waves at grazing angle of incidence is well predicted by the Khokhlov–Zabolotskaya–Kuznetsov equation; even very weakly nonlinear acoustic waves, at grazing angles of incidence, can undergo a nonlinear merging resulting in the formation of a central Mach stem (Marchiano *et al.* 2007). As demonstrated in figure 5, the upstream-propagating waves generated by an impinging jet can be shock-like from their inception, meaning that they easily surpass the criteria for the formation of a central Mach stem at these angles of incidence (Karzova *et al.* 2015).

We have seen examples thus far of duct-like waves, freestream waves, coalescence of multiple weak waves, and merging of shock-like waves. At what impingement conditions do these occur? Regrettably, no simple parametric map appears to be possible, as a jet operating at a single condition can, over a short period of time, produce single waves, double waves that coalesce, and double waves that do not coalesce. Examples of single waves and distinct double waves are provided in figure 9; all four images presented here

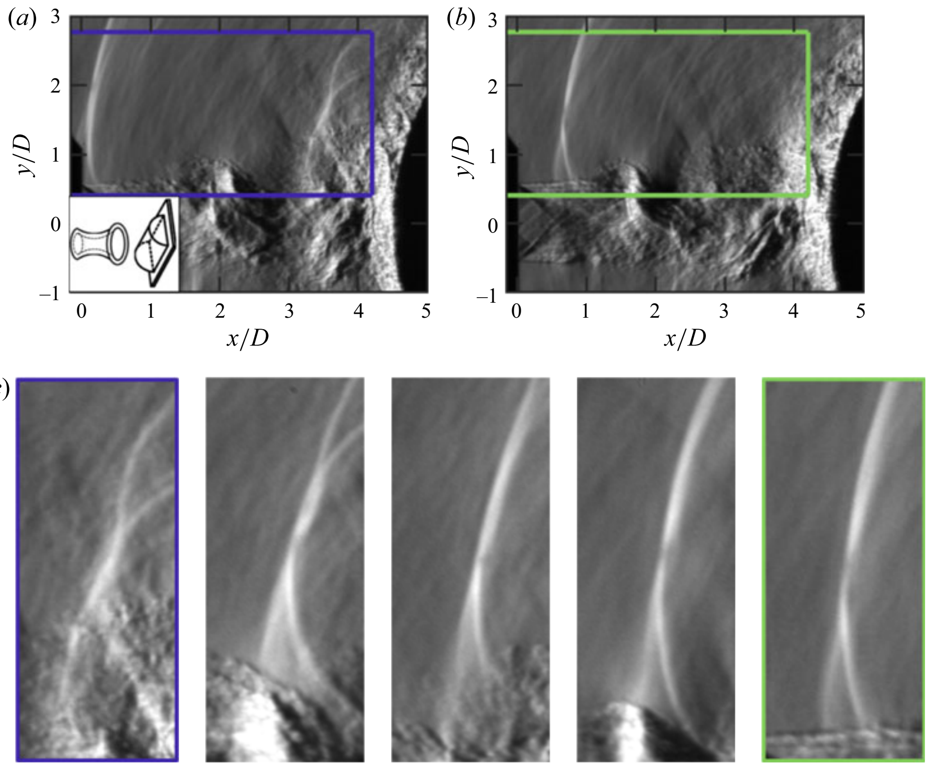

Figure 8. Exemplar image sequence for nonlinear wave coalescence, images spaced by 33 µs, with $NPR = 4.8$, $z/D = 4.5$, $Re = 8.6 \times 10^5$. The directory including exemplar image sequences for this figure and the accompanying Jupyter notebook can be accessed at https://www.cambridge.org/S0022112025103832/JFM-Notebooks/files/Figure8/Figure8.ipynb.

are taken from the same jet at $NPR = 2.5$ striking a cylindrical surface at $z/D = 3.0$. For other conditions, such as that presented in figure 7, both initially shock-like and initially diffuse upstream-propagating waves were observed. Shock-like waves were observed at both the low and high ends of the *NPR* range considered here, and for impingement over a range of distances from the nozzle. While a direct link between the nature of the upstream-propagating wave and the impingement conditions is appealing, at least in these data, nature appears uncooperative. Nonetheless, we have classified one key set of ingredients for resonance, in the form of the various different ways that the loop can be closed by upstream-propagating waves. We now turn our attention to the mechanisms by which these diverse waves are generated.

4. Generation mechanisms

We have demonstrated that the upstream-propagating wave can take a number of forms: duct-like, freestream, steepening, merging. In doing so, we have clarified the nature of the upstream propagation of energy, which is one of the necessary components of a resonance process. Now we seek to bring similar clarity to another component of resonance, in the downstream reflection point: what is the birthplace of these various upstream-propagating waves? In this section, we seek to identify at least some of the mechanisms at work, and where possible, to connect them to the resultant waveforms. To recapitulate the summary in § 1, there is some mechanism associated simply with the arrival of a vortex at a solid surface, with the flat plate acting to reflect some of that energy upwards. There is a

https://doi.org/10.1017/jfm.2025.10383 Published online by Cambridge University Press

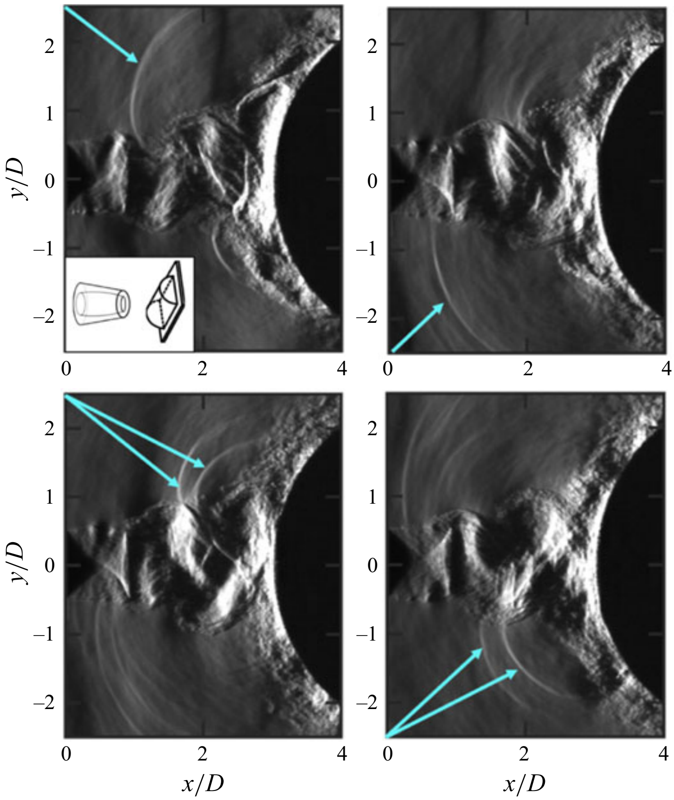

Figure 9. Examples of both single and double nonlinear waveforms generated at the same operating conditions: $NPR = 2.50$, $z/D = 3.0$, $Re = 5.9 \times 10^5$. The directory including exemplar image sequences for this figure and the accompanying Jupyter notebook can be accessed at https://www.cambridge.org/S0022112025103832/JFM-Notebooks/files/Figure9/Figure9.ipynb.

proposed mechanism associated with the fluctuation of the wall-jet boundary, where said boundary acts like a 'membrane', and the sound is generated by a bulk upstream motion of mass. There is a proposed mechanism associated with a transient wall-jet shocklet. Finally, though not explicitly discussed in prior literature, a shock-leakage-like mechanism has been observed in prior work (Weightman *et al.* 2019).

4.1. *Vortex sound*

We first address the generation mechanism associated with the arrival of vortices at the wall, though with the caveat that we will not present new data here, but only attempt to summarise existing research, and contextualise it in terms of new knowledge. The sound generated through the interaction of an isolated vortex ring with a solid wall has been studied in detail (Kontis *et al.* 2008), and is generally well predicted by the theory of vortex sound (Howe 2003). An axisymmetric vortex ring impinging upon a wall produces sound of a quadrupolar nature (Nakashima & Inoue 2008), with the quadrupole aligned such that the directions of maximum radiation are normal and tangential to the wall, centred on the vortex core. While the shear-layer vortices associated with the KH wavepacket are not identical to an isolated vortex ring, their pressure distribution is similar, with an $m = 0$ wavepacket producing peak pressure fluctuations at the centreline of the jet (Tam & Hu 1989). The closest analogy is a compressible vortex ring generated from a shock tube, which carries a trailing jet rather than being an isolated structure. The impact of such a structure on a solid wall produces a pressure maximum at the centreline of the vortex ring (Minota, Nishida & Lee 1997), behaviour that is also observed in the collision of two compressible vortices at a plane of symmetry (Minota, Nishida & Lee 1998), equivalent to the collision of a vortex ring with an inviscid wall. Thus it is reasonable to hypothesise that the mechanism of vortex sound will produce an effective source at the core of the jet.

The fact that the source is located within the core of the jet, in the context of recent work, explains why the upstream-propagating waves associated with this mechanism are either duct-like for subsonic jets (Tam & Ahuja 1990; Varé & Bogey 2022*a*) or associated with the radially extended guided jet mode for supersonic jets (Tam & Norum 1992; Varé & Bogey 2023). Nogueira *et al.* (2024) demonstrated that for a given range of frequencies, sound generated in the core of the jet will undergo reflection and transmission processes at the shear layer that will produce an upstream-propagating wave that is either duct-like (when total reflection occurs) or decays exponentially in the radial direction (the previously named guided jet mode). This is, in fact, the only mechanism by which acoustic waves generated in the core of the jet can propagate upstream. We thus have an explanation for why in some regimes resonance predictions based on the bands of existence of the guided jet mode produce exceptionally robust predictions and explanations of impinging jet resonance (Varé & Bogey 2023). Further, as mentioned in § 1, for these same conditions, predictions of sound based on Curle's analogy match closely with the simulation data, which supports the argument that vortex sound is the relevant mechanism for these flows.

To summarise, we thus hypothesise that when the dominant mechanism of sound production is vortex sound, the upstream-propagating wave will be the so-called guided jet mode, i.e. a finite-frequency-band internal reflection and transmission of acoustic waves generated in the jet core near the wall. We note also that the collision of even subsonic compressible vortex rings can produce waves of sufficient amplitude and nonlinearity to be classified as shocks, rather than acoustic waves, as demonstrated in Minota *et al.* (1998) and more recently in Bauer *et al.* (2022). The impact of the vortex upon the impingement surface is thus a candidate for producing some of the shock-like waves observed in § 3. It is not immediately apparent whether a weak shock generated within the jet could only propagate upstream for the finite-frequency range predicted by the model of Nogueira *et al.* (2024); the model is linear and thus assumes waves of infinitesimal amplitude. Nonetheless, though these waves are strong for acoustic waves, they are still very weak for shock waves, thus we assume that the frequency constraints suggested by the linear model should hold in at least a qualitative sense.

The direct interaction of the vortex with the wall is not the only mechanism by which acoustic waves may be generated, however, particularly when the incoming jet is supersonic. We turn now to other potential mechanisms.

4.2. *Wall-jet shocklet*

We commence our discussion of other mechanisms by revisiting the wall-jet shocklet phenomenon first discovered in Weightman *et al.* (2017*b*). Then, as now, the shocklet was challenging to visualise, as it is located within the highly turbulent wall jet, and exists for only tens of microseconds at a time. Nonetheless, in figure 10 we present some new shadowgraph visualisations of the shocklet, obtained by using a rectangular jet impinging on a cylindrical surface. The data here are consistent with the explanation in Weightman *et al.* (2017*b*): the large vortex associated with the KH wavepacket moves from the primary jet to the wall jet, and in doing so generates a transient shock structure in the wall jet. As the vortex convects further down the wall and removes the imposed velocity field, the

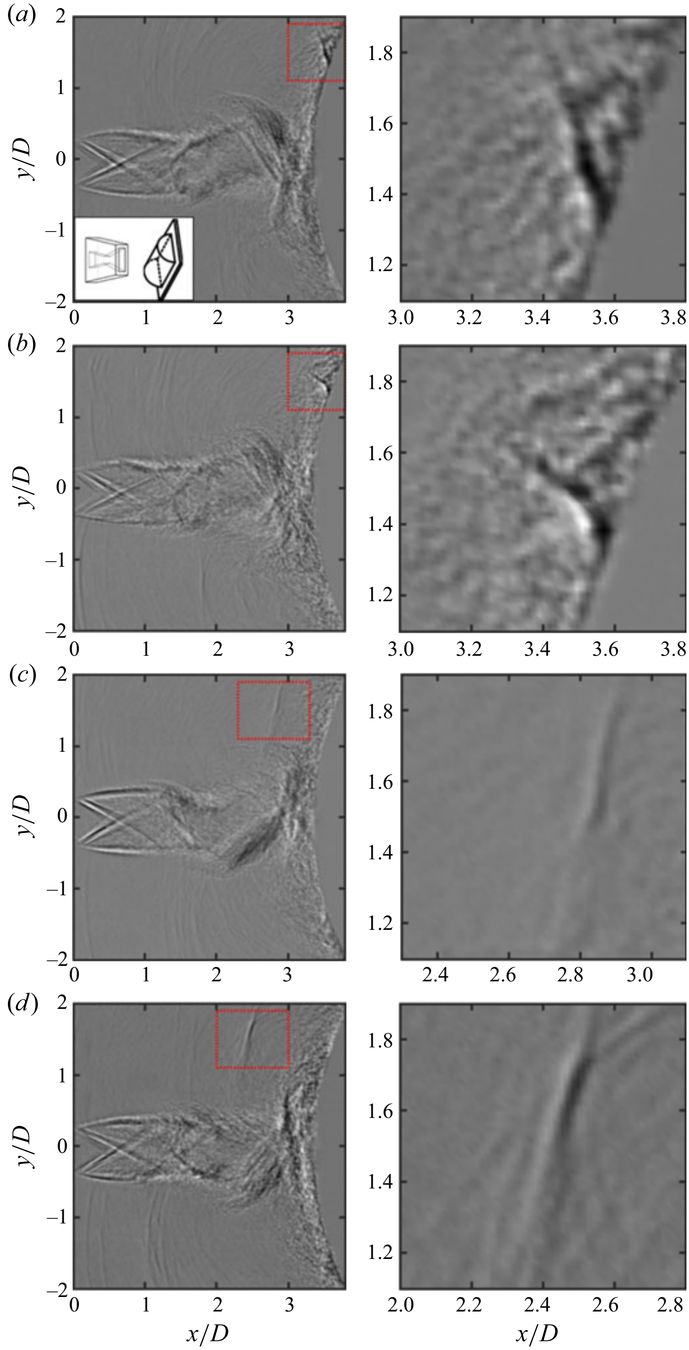

Figure 10. Image sequence showing full-field and magnified shadowgraph of a shocklet in the wall jet generating an upstream propagating wave, with $NPR = 5.5$, $z/D = 3.5$, $Re = 7.8 \times 10^5$. The directory including exemplar image sequences for this figure and the accompanying Jupyter notebook can be accessed at https://www.cambridge.org/S0022112025103832/JFM-Notebooks/files/Figure10/Figure10.ipynb.

shocklet moves upstream, generating a nonlinear compression wave. Figure 10(*a*) shows the shocklet forming as the vortex moves past, and figure 10(*b*) shows the retrograde tilting of the shocklet as the vortex moves away. The resultant nonlinear upstream-propagating wave is visible in figures 10(*c*) and 10(*d*).

Though the mechanism described here does not differ from that in Weightman *et al.* (2017*b*), the new data herein have the advantage that they span a much larger range of operating conditions and nozzle and surface geometries. The location of the shocklet, and the degree of motion that it experiences, are observed to be highly case dependent. A general trend is that the shocklet moves radially from the jet with increasing Mach number. It is, in fact, not visible in most datasets for lower pressure ($NPR \leq 3.0$), but this does not mean that it is not present; it is simply that the turbulent wall jet so obscures this region that its presence or lack thereof cannot be determined. There are also many cases where the shocklet is visible in the images, but is not observed to undergo the tilting motion responsible for the production of acoustic waves. With the caveat that the flow is complex, and the relative strength of waves cannot be rigorously determined from schlieren images, in the present dataset it appears that the wall-jet shocklet is consistently responsible for the upstream-propagating wave that closes resonance when $NPR \geq 4.5$ and $z/D \leq 4.0$. Given what is known of the mechanism underpinning the wall-jet shocklet, it is reasonable to propose that the likely condition for its existence is that the wall jet fluctuates between supersonic and subsonic with the passage of large-scale vortices. With some caution, we hypothesise that the wall-jet shocklet as a mechanism for sound production plays no role in resonance for subsonic and low-Mach supersonic jets, and an increasing role as jet Mach number increases. We also suggest that the shocklet might be observed for lower *NPR* when the jet impinges onto a curved surface, as the wall jet will maintain a higher mean velocity in these cases. However, in the present data we also find the shocklet producing the upstream-propagating wave in the case of impingement upon a flat plate.

Critically, the shocklet generates the upstream-propagating wave well outside the jet core. Thus the frequency-dependent nature of the guided jet mode is irrelevant here; the guided jet mode only governs sound waves that originate from within the core of the jet (Nogueira *et al.* 2024). The shocklet also generates waves that are sharp and nonlinear from their inception; at the moment of its birth, the wave is actually a shock, and only through diffraction does it decay to something that might be more appropriately described as a nonlinear acoustic wave, acknowledging that the difference between the two is only a matter of degree. This shocklet thus provides a possible generation mechanism for the initially sharp waves observed § 3.

4.3. *Shock leakage*

The wall-jet shocklet is not the only shock-related mechanism for the production of sound, however. As detailed in § 1, the wall-jet shocklet shares many properties with the shock-leakage phenomenon identified in screeching jets (Edgington-Mitchell *et al.* 2021); both mechanisms involve the unsteady motion of a shock under the action of a transient velocity field induced by the passage of a vortex. The authors of this paper, as well as others (Gojon & Bogey 2017), have for some time hypothesised that shock leakage should be active at the stand-off shock in supersonic jets, and indeed calculations based on the ray-tracing model of Shariff & Manning (2013) using experimentally derived velocity fields support this hypothesis, though they have not yet been published. Indeed, such a mechanism was observed in the high-fidelity numerical simulations of Varé & Bogey (2022*b*), who recognised it as the same mechanism active in screeching jets. In their data, the phenomenon was observed to produce strong nonlinear upstream propagating waves at some conditions, but not at others. In the present dataset, we identify multiple conditions where upstream-propagating waves do indeed appear to be generated by a shock-leakage mechanism. Before presenting some of these examples, we must acknowledge a significant limitation in the nature of schlieren imaging, and thus place a caveat on the discussion to follow. As described in § 4.1, the collision of a vortex ring with a wall can produce not only acoustic waves, but a shock wave that travels retrograde to the motion of the vortex. If such a mechanism is active in these impinging jets (and it likely is for many operating conditions), then an upstream-propagating shock may well be generated within the core of the jet. The arrival of this wave at the stand-off shock will displace the stand-off shock, and this displacement may, from the perspective of a schlieren image, manifest in a similar manner to shock leakage. Given that the turbulent wall jet prevents direct observation of where the vortex impacts the wall, we cannot categorically state whether in all cases the motion of the stand-off shock that we observe is driven by the passage of downstream-propagating vortices, or the arrival of upstream-propagating shocks. There are, however, cases where the stand-off shock is sufficiently far from the wall that shock leakage can be observed before the vortex arrives at the wall. The model of Shariff & Manning (2013), which dictates that the primary determinant of shock leakage is the strength of the imposed vorticity field, predicts that significant leakage will occur for the PIV data previously presented in Weightman *et al.* (2017*b*, 2019). Which mechanism is dominant is beyond the scope of the present work, and it may even be that the two mechanisms are synchronised.

With these caveats in mind, we turn to our first example, presented in figure 11. In an attempt to render the phenomenon clearly, we combine three different imaging approaches here: schlieren of the $\partial\rho/\partial x$ gradient, shadowgraph, and an *a posteriori* correlation-based phase average of the shadowgraph. Note here that the schlieren and shadowgraph were not taken simultaneously, and have been manually phase matched. The generation of a single upstream-propagating wave, produced by a rectangular jet impinging on a cylinder, is shown in images separated by 20 μs; the cyan arrow indicates the wave in question, and the magenta arrow indicates the vortex responsible for its production. Figure 11(*a*) shows the initial leakage of the wave, which occurs just after the passage of the large KH vortex, consistent with the phenomenon observed in screeching jets (Edgington-Mitchell *et al.* 2021). Figure 11(*b*) presents two slightly different manifestations of the shock-leakage process; a single contiguous upstream wave is visible in the schlieren, whereas in the shadowgraph (and more clearly in the phase-averaged version), a discontinuity is evident between segments of the upstream-travelling wave. This particular manifestation, which is visible in the present data at many different operating conditions, is a form of shock leakage that has not been observed in screeching jets to the best of our knowledge. The resonance process in impinging jets is much stronger than that observed in screeching jets, with the higher-amplitude forcing producing KH vortices that grow much more rapidly. Given the relationship between vortex strength and shock leakage (Suzuki & Lele 2003), this will result in a much larger rotation of the wavefront normal of the section of shock that 'leaks'. We see the effects of this stronger rotation here: part of the shock has actually been rotated so strongly that it is directed back towards the core of the jet. The discontinuity between the two wave segments is divided into regions where the wave is freely propagating in near-quiescent fluid, and where it is propagating through the shear layer of the jet (thus moving more slowly in the laboratory-fixed reference frame). By figure 11(*c*), the inner portion of the wave has been transmitted into the jet itself, leaving only the outer portion to continue propagating upstream. Figure 11(*d*) shows the commencement of a new shock-leakage process on the lower side of the jet, as the wave on the upper side continues towards the nozzle.

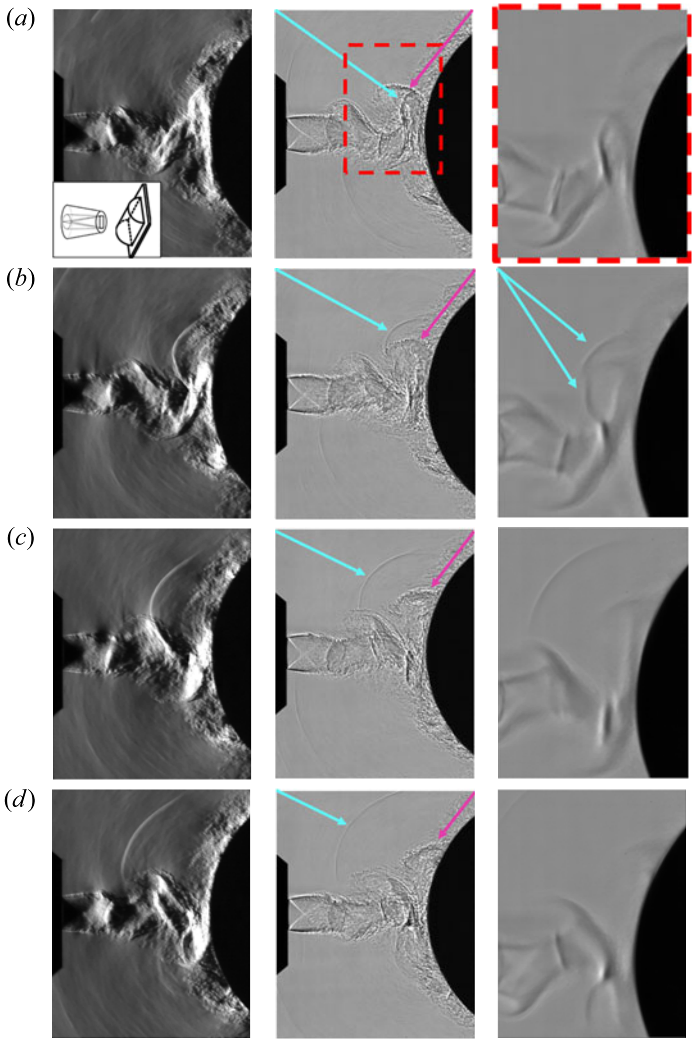

Figure 11. Visualisation of the shock-leakage phenomenon. Left: $\partial\rho/\partial x$ schlieren. Centre: shadowgraph. Right: phase-averaged shadowgraph. Here, $NPR = 3.4$, $z/D = 3.0$, $Re = 6.0 \times 10^5$. The directory including exemplar image sequences for this figure and the accompanying Jupyter notebook can be accessed at https://www.cambridge.org/S0022112025103832/JFM-Notebooks/files/Figure11/Figure11.ipynb.

4.4. *Dual mechanisms*

With three distinct mechanisms of upstream-wave generation identified, all of which are capable of producing the sharp nonlinear waveforms observed in figure 2(*b*), we now seek to explain the various manifestations of double-wave phenomena: pairs of waves that either merge (figure 2*c*) or remain separate (figure 9). All three mechanisms are linked to the action of the large vortical structures that comprise the downstream-propagating portion of the resonance loop. In the case of vortex sound, it is the interaction of the vortices themselves with the wall that produces the upstream wave, whereas for shock leakage, it is the interaction with the stand-off shock, and for the shocklet, with the wall jet. As all three mechanisms are linked to the same vortical structure, it is reasonable to assume that there may be situations where more than one of these mechanisms is active. The vortex-sound mechanism should always produce an upstream-propagating wave if the

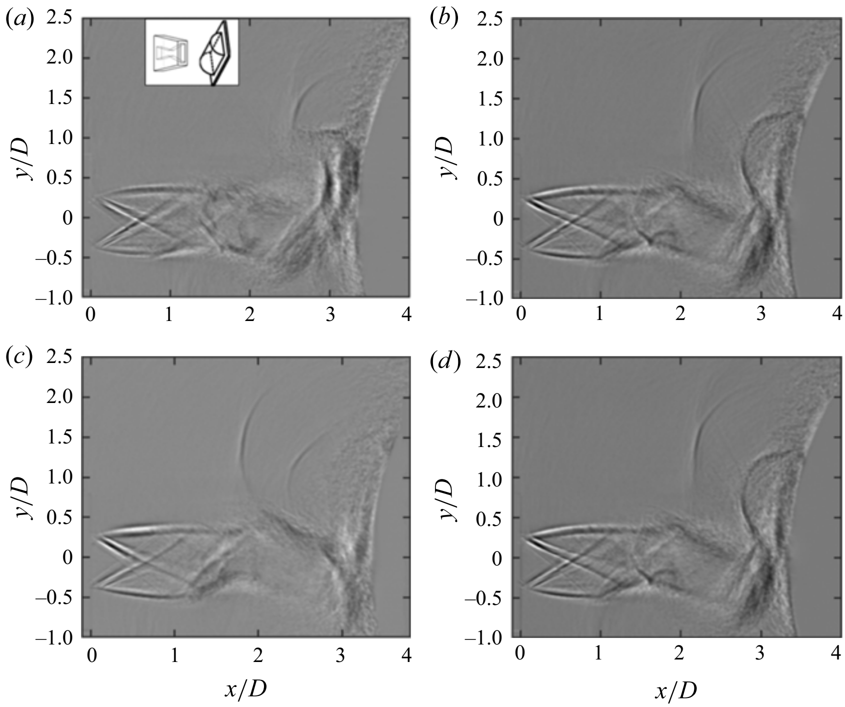

Figure 12. Phase-averaged shadowgraph showing the two separate mechanisms generating upstream-propagating waves in a single period of the resonance cycle, with $NPR = 5.5$, $z/D = 3.5$, $Re = 7.8 \times 10^5$. The directory including exemplar image sequences for this figure and the accompanying Jupyter notebook can be accessed at https://www.cambridge.org/S0022112025103832/JFM-Notebooks/files/Figure12/Figure12.ipynb.

induced velocity field of the vortex is influenced by the wall; the degree to which the vortex interacts with the wall will be governed by how far from the wall the mean flow develops a significant non-streamwise velocity component, which in turn is highly dependent on jet Mach number and impingement height. The shock-leakage mechanism is known to depend primarily on the strength of the vorticity fluctuations in the shear layer, but in impinging jets, the structure of the stand-off shock, annular or otherwise, likely also plays a role. The exact requirements for the shocklet to generate upstream waves remain unclear, but seem to be linked to both the strength of the vortical structure and the speed of the wall jet.

Figure 12 shows an exemplar sequence of phase-averaged shadowgraph images, whereby two discrete upstream-propagating waves are generated as part of the impingement cycle. The first wave, produced by a shocklet in the wall jet, is visible in figure 12(*a*); note that this wave was not actually produced by the vortex visible near the impingement surface, but was produced by its predecessor. This phenomenon, whereby two closely spaced waves can be generated by separate vortices, is observed for a range of operating conditions. Figure 12(*b*) shows the genesis of the second wave, a shock-like wave that is either the result of a shock-leakage process or the nonlinear wave resulting from the vortex interacting with the wall. figures 12(*c*) and 12(*d*) show the waves propagating upstream, with slightly different directionality, and a significant space between them.

Having considered a case where dual mechanisms generate pairs of waves with significant spatial separation, we now consider the same geometry with only a slight increase in back pressure, and observe a phenomenon at the opposite extreme, where two

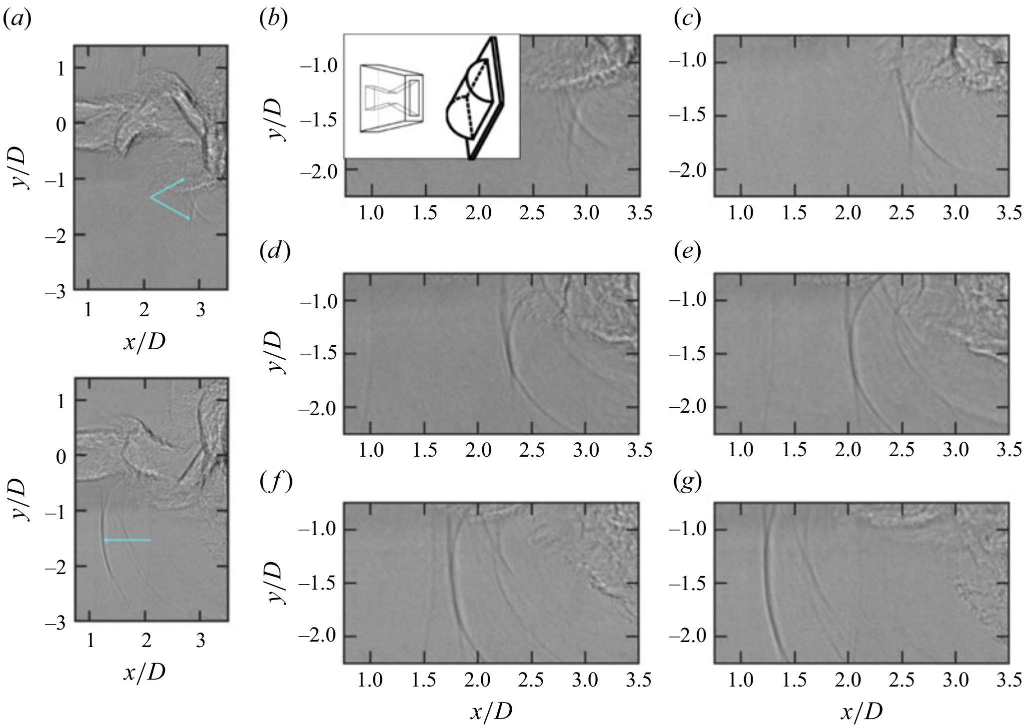

Figure 13. Shadowgraph showing merging of two initially nonlinear waves from spatially distinct sources, with $NPR = 6$, $z/D = 3.5$, $Re = 8.5 \times 10^5$. The directory including exemplar image sequences for this figure and the accompanying Jupyter notebook can be accessed at https://www.cambridge.org/S0022112025103832/JFM-Notebooks/files/Figure13/Figure13.ipynb.

mechanisms generate waves that merge. The shadowgraph images in figure 13 show two discrete waves generated at different points in the wall jet: one with an origin at $y/D \approx -2$ produced by a shocklet, and another at $y/D \approx -1$ that is likely the product of either another shocklet, or a vortex-sound mechanism. Tracking the wave in figure 13(*b–g*), the same merging process observed in figure 8 is evident. Here, we thus have our explanation for the merging phenomenon (Willis *et al.* 2023) observed in those earlier figures: two separate waves are produced by different mechanisms, and in fact are associated with different vortices in a given resonance cycle. At some flow conditions, as in figure 12, these waves remain distinct, while at others, such as in figure 13, they merge into a single waveform of even higher amplitude.

The previous two phenomena (merging and non-merging waves) were observed at different pressure ratios. This might give rise to some hope that synchronisation of the waves depends in a straightforward manner on the jet Mach number. Regrettably, the flow continues to resist such straightforward classification; figure 14 shows that even at a single operating condition, waves can be observed remaining distinct, as in figure 14(*a,c*), or merging, as in figure 14(*b,d*). It is reasonable to imagine that if there is some phase delay between the production of the two waves, there should be a specific frequency at which these waves merge. In practice, however, these are highly turbulent flows, and the stochastic nature of the turbulence produces sufficient jitter in the phase and amplitude of the KH wavepacket that there is in fact a range of frequencies where merging may or may not be observed for a given resonance cycle. While our discussion has focused on how the waves behave as they move back towards the nozzle (indicated with a cyan

https://doi.org/10.1017/jfm.2025.10383 Published online by Cambridge University Press

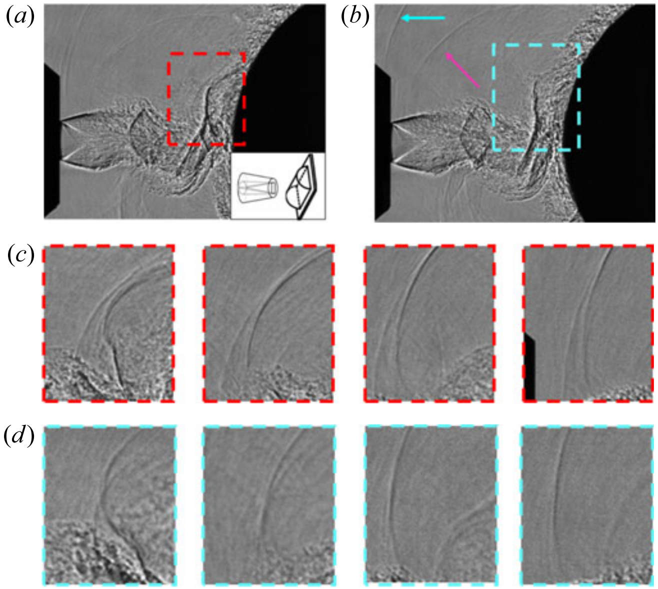

Figure 14. Demonstration that waves generated by two mechanisms can (*a*,*c*) remain separate, (*b*,*d*) merge, with $NPR = 3.8$, $z/D = 3.0$, $Re = 6.7 \times 10^5$. The directory including exemplar image sequences for this figure and the accompanying Jupyter notebook can be accessed at https://www.cambridge.org/S0022112025103832/JFM-Notebooks/files/Figure14/Figure14.ipynb.

arrow), looking outside the coloured boxes in figures 14(*a*) and 14(*b*) reveals what appears to be an additional wave (indicated by the magenta arrow); there are two distinct upstream-propagating waves by the time we reach the nozzle. One of these waves (cyan) has resulted from the merging process of two waves as depicted in figure 14(*d*): the magenta wave appears to have a different origin, a different direction of propagation, and a clear spatial separation from the merged or unmerged wave pair. This wave will be the subject of our final proposed mechanism, which is, in the view of the authors, perhaps the most intriguing, but also the hardest to clearly visualise.

To study this final mechanism, we consider a series of shadowgraph images for an axisymmetric jet impinging upon the hemispherical surface, presented in figure 15. Figures 15(*a*) and 15(*b*) represent the initial and final states that we will consider; figure 15(*a*) is the beginning of a shock-leakage process on the lower half ($-y$) side of the jet, while figure 15(*b*) is the production of two discrete waves on the upper side ($+y$) side of the jet. Figure 15(*c*–*g*) are an *a posteriori* phase average based on a region of interest that moves with the wave in question; this is thus not a true phase average, but a *post hoc* phase average that has been constructed to emphasise particular features. The motivation for so doing is that while some phenomena appear quite clear when animated, they are difficult to identify in a series of still frames; the raw videos without phase averaging are provided in supplementary movie 11. The images in figures 15(*a*) and 15(*c*) show that as the initial shock-leakage event on the $-y$ side of the jet takes place, part of the wave (labelled in magenta) is rotated sufficiently that it propagates back into the jet, rather than towards the nozzle. This portion of the wave travels towards the jet centreline above the stand-off shock, until it reaches a region where the retrograde flow exceeds the speed of sound, typically a nascent oblique shock, and merges with this shock. In some configurations, components of this wave are observed to exit the jet on the other side, though in many cases, the timing is such that no component of this transverse wave can

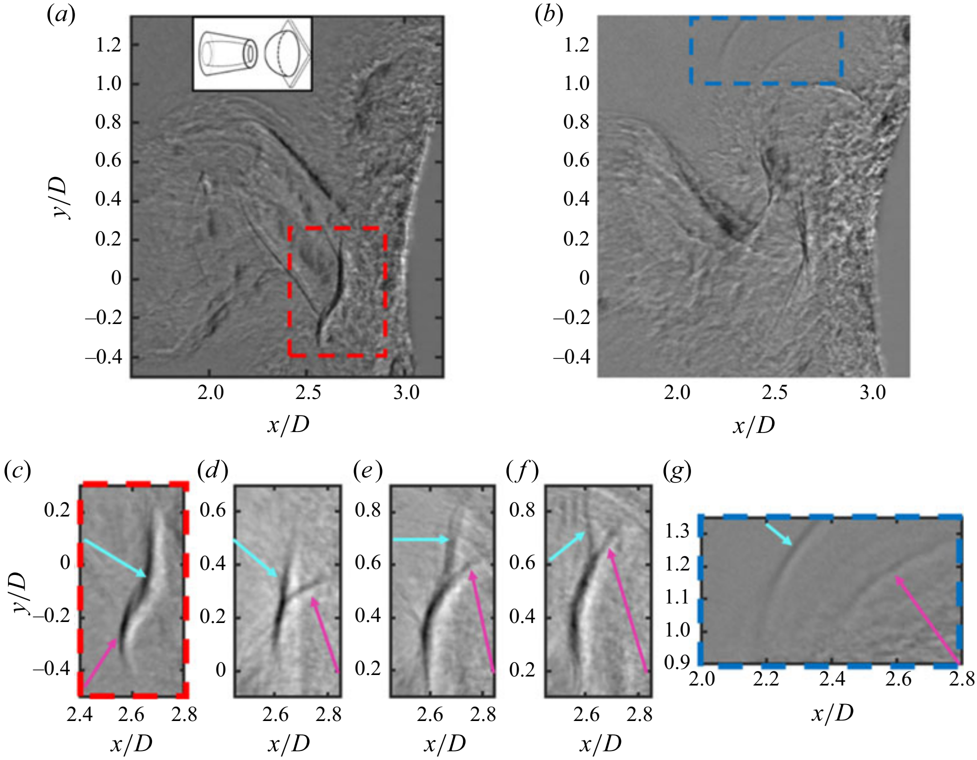

Figure 15. (*a*) Initial and (*b*) final shadowgraph images showing the production of a double nonlinear freestream wave. (*c–g*) A sequence of *a posteriori* phase-averaged shadowgraphs, with the two components of the wave described in the text indicated by cyan and magenta arrows. Here, $NPR = 2.5$, $z/D = 3.0$, $Re = 5.9 \times 10^5$. The directory including exemplar image sequences for this figure and the accompanying Jupyter notebook can be accessed at https://www.cambridge.org/S0022112025103832/JFM-Notebooks/files/Figure15/Figure15.ipynb.

cross the jet above the stand-off shock. Our focus here instead is the portion of this wave that moves below the stand-off shock, in the region where the flow is subsonic. That this wave exists at all is surprising; the wavefront normal is rotated almost at right angles to its undisturbed shape, as shown in figure 15(*d*). By figure 15(*e*), the arrival of a vortex on the $+y$ side of the jet has begun the motion of the shock (in cyan) that will shortly produce another upstream-propagating wave by way of shock leakage. The transverse wave is close but measurably lagging the new wave associated with shock leakage, still completing its transverse motion as the section of shock indicated in cyan begins to move upstream in figure 15(*f*). Finally, in figure 15(*g*), the two discrete waves are seen moving upstream; leading the way is the more recently produced wave from the $+y$ side, while close behind is a wave whose provenance was on the $-y$ side of the jet. The final directivity of these waves is quite different; the transverse wave is strongest in the radial direction, while the shock leakage process sends strong waves directly back upstream towards the nozzle.

In § 3, we identified five distinct families of upstream-propagating waves: duct-like, single nonlinear freestream, double nonlinear freestream, merging nonlinear waves, and coalescing diffuse waves. We have now proposed generation mechanisms for all of these bar the last. We also have not directly linked the mechanism described in Henderson *et al.* (2005), i.e. the bulk motion of the wall jet acting as a mass displacement and thus sound source, to any of these waves. The nature of the present data precludes us from conclusively demonstrating a link between the two, but we nonetheless hypothesise that these diffuse waves could be produced by a large-scale displacement of the wall jet rather than the highly localised shock-associated sources discussed earlier. The data in Henderson *et al.* (2005) suggest that the movement of the wall-jet boundary is subsonic relative to the ambient air, meaning that the resultant waves would not be shock-like. The displacement of the boundary is also going to be distributed over a non-compact region on the surface of the wall, meaning that the source of the wave will also be distributed. Thus while we cannot demonstrate it categorically, large displacements of the wall jet have the necessary characteristics to be responsible for the generation of these diffuse collections of weaker upstream-propagating waves, which then coalesce into a single nonlinear wave.

On a final note, we have observed a number of configurations where two strong waves are produced by the passage of a single vortical structure. This presents something of a challenge for the traditional model of resonance in such a flow: two upstream-propagating waves transferring energy to the jet shear layer near the nozzle should in turn produce two vortical structures, not one. Though interpretation is complicated by path-integration effects, in many cases where dual waves were observed, only one of the two was observed to interact with the shear layer near the nozzle, with either the other not reaching the nozzle at all, or only a weak component of the wave reaching the nozzle. There are a few select cases where some form of complicated amplitude modulation appeared to be taking place, which could suggest a more complex feedback process, but in the majority of cases, if two waves exist and did not merge, only one was involved in resonance.

5. Conclusions

There has been some historical dissonance between the assumptions of models for impinging-jet resonance and the waves observed in experiments. Multiple researchers have demonstrated excellent frequency prediction using models that assume that the upstream-propagating wave is the guided jet wave, a wave that is now known to be the result of reflection and transmission of sound generated inside the jet itself. Conversely, multiple experiments have observed the production of upstream-propagating waves from the wall jet, well outside the core of the primary jet. In this paper, we show that there are multiple mechanisms by which the upstream-propagating waves can be generated, and multiple forms that they can take. If we place ourselves in a Lagrangian reference frame bound to a vortex that has arisen from the Kelvin–Helmholtz instability, as we reach the region of flow near the impingement surface, we will have four opportunities to witness the production of upstream-waves.

(i) Chronologically, our first opportunity comes through the mechanism of shock leakage (Manning & Lele 2000), as we pass the stand-off shock. Here, the strong vorticity associated with the very large vortices present in resonating impinging jets can produce significant distortions of this shock in the shear layer. These distortions permit some of the shock to leak out into the freestream, whereupon it propagates back towards the nozzle. The waves associated with this mechanism are shock-like from their moment of inception.

(ii) Our second mechanism involves an interaction between the pressure field associated with the vortex and the impingement surface itself. Well-validated theories exist to predict that this interaction produces sound with distinctive characteristics (Howe 2003), and this has been demonstrated quantitatively for impinging jets using Curle's analogy (Varé & Bogey 2022*a*). While in the past this interaction has been discussed as a mechanism for producing acoustic waves, in the case of compressible vortex rings interacting with a surface, the resulting waves can be nonlinear and even shock-like. In this work, we demonstrate that the duct-like modes produced by this mechanism can also be highly nonlinear, bearing a remarkable resemblance to the shock structures in a free underexpanded jet.

(iii) As the pressure field associated with the vortex interacts with the plate, the vortex itself is deflected away from the jet, following the shape of the mean flow, which turns outwards away from the jet centreline. As the vortex moves into the wall jet, it induces significant fluctuations in the wall jet; in many of the cases observed here, the vortex itself is significantly larger than the thickness of the wall jet. In the mechanism proposed by Henderson *et al.* (2005), these fluctuations induce upstream motions in the boundary of the wall jet, which creates sound analogous to the movement of a membrane. Though difficult to quantify in the present data, we hypothesise that such a mechanism is consistent with the production of relatively linear acoustic waves from distributed sources, which then can be observed to coalesce into a single more strongly nonlinear wave during their upstream propagation.

(iv) Our final mechanism arises again from the interaction between our vortex and the wall jet, but is of rather different character. For impingement surfaces that are sufficiently close to the nozzle, or for sufficiently high-speed jets, the wall jet may be transonic or supersonic. The induced velocity field of the vortex, which is once again very large relative to the wall jet, is sufficient to produce transient shocklets embedded in the wall jet. As the vortex moves away, and removes its induced velocity field, the shocklets must begin to translate themselves to satisfy the shock-jump conditions; this results in elements of the shocklet propagating back towards the nozzle in the form of a nonlinear wave.

We have also demonstrated that these mechanisms can coexist, meaning that the upstream-propagating wave can be linear or nonlinear, singular or in pairs, and these pairs can travel separately or merge together. In some cases, strong waves are observed that do not reach the nozzle, meaning that the sound measured at some observer positions may include strong tonal components that are not actually involved in the resonance process, but are a by-product of it.

Despite a thorough analysis of an extensive dataset, we have been unable to identify clear relationships between these four mechanisms and the Mach number of the jet or the azimuthal mode (or rectangular equivalent) of the resonance loop. The shocklet mechanism appears to strengthen at higher jet Mach numbers and shorter impingement distances, and the effective source of the upstream-propagating waves moves radially outwards as the jet Mach number increases. These are only observations of general trends, however; increasing Mach number can instead switch the resonance cycle off completely, as documented in Henderson (2002), and at this point there is no reason to think that the other mechanisms would weaken at higher Mach numbers.

The various mechanisms and their complex relationship with the parameters of the impinging-jet system mean that for now, a complete description of the physics remains out of reach. Nonetheless, in this work we have at least demonstrated that the two seemingly contradictory approaches to resonance in these systems are in fact not in contradiction, but simply addressing different mechanisms that can form part of the resonant feedback loop.

Supplementary material. Computational Notebook files are available as supplementary material at https://doi.org/10.1017/jfm.2025.10383 and online at https://www.cambridge.org/S0022112025103832/JFM-Notebooks.

Funding. D.E.-M. and P.N. were supported by the Australian Research Council through the Future Fellow scheme (FT220100679) and DECRA scheme (DE240100933), respectively. Our gratitude to former laboratory member Ms R. Kirby for the outstanding colour schlieren visualisation in figure 1.

Declaration of interests. The authors report no conflict of interest.

References

Baars, W.J., Tinney, C.E., Wochner, M.S. & Hamilton, M.F. 2014 On cumulative nonlinear acoustic waveform distortions from high-speed jets. *J. Fluid Mech.* **749**, 331–366.

Bauer, R.L., Thomas, C.J., Baker, E.V.P., Johnson, E.M., Williams, K.R., Langenderfer, M.J. & Johnson, C.E. 2022 Shock wave formation from head-on collision of two subsonic vortex rings. *Sci. Rep.* **12** (1), 7492.

Bogey, C. & Gojon, R. 2017 Feedback loop and upwind-propagating waves in ideally expanded supersonic impinging round jets. *J. Fluid Mech.* **823**, 562–591.

Edgington-Mitchell, D. 2019 Aeroacoustic resonance and self-excitation in screeching and impinging supersonic jets – a review. *Intl J. Aeroacoust.* **18** (2–3), 118–188.

Edgington-Mitchell, D., Jaunet, V., Jordan, P., Towne, A., Soria, J. & Honnery, D. 2018 Upstream-travelling acoustic jet modes as a closure mechanism for screech. *J. Fluid Mech.* **855**, R1.

Edgington-Mitchell, D., Li, X., Liu, N., He, F., Wong, T.Y., Mackenzie, J. & Nogueira, P. 2022 A unifying theory of jet screech. *J. Fluid Mech.* **945**, A8.

Edgington-Mitchell, D., Weightman, J., Lock, S., Kirby, R., Nair, V., Soria, J. & Honnery, D. 2021 The generation of screech tones by shock leakage. *J. Fluid Mech.* **908**, A46.

Edgington-Mitchell, D.M., Weightman, J. & Nogueira, P.A.S. 2024 Mechanisms of tone generation in impinging supersonic jets. In *30th AIAA/CEAS Aeroacoustics Conference*, AIAA Paper 2024-3375, p. 3375.

Ferreira, F., Fiore, M., Parisot-Dupuis, H. & Gojon, R. 2023 Neutral acoustic wave modes in supersonic impinging jets. *AIAA J.* **61** (2), 955–964.

Fiévet, R., Tinney, C.E., Baars, W.J. & Hamilton, M.F. 2016 Coalescence in the sound field of a laboratory-scale supersonic jet. *AIAA J.* **54** (1), 254–265.

Gee, K.L., Sparrow, V.W., James, M.M., Downing, J.M., Hobbs, C.M., Gabrielson, T.B. & Atchley, A.A. 2008 The role of nonlinear effects in the propagation of noise from high-power jet aircraft. *J. Acoust. Soc. Am.* **123** (6), 4082–4093.

Gojon, R. & Bogey, C. 2017 Flow structure oscillations and tone production in underexpanded impinging round jets. *AIAA J.* **55** (6), 1792–1805.

Gojon, R., Bogey, C. & Marsden, O. 2016 Investigation of tone generation in ideally expanded supersonic planar impinging jets using large-eddy simulation. *J. Fluid Mech.* **808**, 90–115.

Gojon, R., Bogey, C. & Mihaescu, M. 2018 Oscillation modes in screeching jets. *AIAA J.* **56** (7), 1–7.

Hamilton, M.F. & Blackstock, D.T. 2024 *Nonlinear Acoustics*. Springer Nature.

Henderson, B. 2002 The connection between sound production and jet structure of the supersonic impinging jet. *J. Acoust. Soc. Am.* **111** (2), 735–747.

Henderson, B., Bridges, J. & Wernet, M. 2005 An experimental study of the oscillatory flow structure of tone-producing supersonic impinging jets. *J. Fluid Mech.* **542**, 115–137.

Howe, M.S. 2003 *Theory of Vortex Sound*. Cambridge University Press.

Jaunet, V., Mancinelli, M., Jordan, P., Towne, A., Edgington-Mitchell, D.M., Lehnasch, G. & Girard, S. 2019 Dynamics of round jet impingement. In *25th AIAA/CEAS Aeroacoustics Conference*, AIAA Paper AIAA 2019-2769, pp. 2769.

Jordan, P. & Colonius, T. 2013 Wave packets and turbulent jet noise. *Annu. Rev. Fluid Mech.* **45** (1), 173–195.

Jordan, P., Jaunet, V., Towne, A., Cavalieri, A.V.G., Colonius, T., Schmidt, O. & Agarwal, A. 2018 Jet–flap interaction tones. *J. Fluid Mech.* **853**, 333–358.

Karami, S., Edgington-Mitchell, D., Theofilis, V. & Soria, J. 2020*a* Characteristics of acoustic and hydrodynamic waves in under-expanded supersonic impinging jets. *J. Fluid Mech.* **905**, A34.

Karami, S., Stegeman, P.C., Ooi, A., Theofilis, V. & Soria, J. 2020*b* Receptivity characteristics of under-expanded supersonic impinging jets. *J. Fluid Mech.* **889**, A27.

Karzova, M.M., Khokhlova, V.A., Salze, E., Ollivier, S. & Blanc-Benon, P. 2015 Mach stem formation in reflection and focusing of weak shock acoustic pulses. *J. Acoust. Soc. Am.* **137** (6), EL436–EL442.

Kontis, K., An, R., Zare-Behtash, H. & Kounadis, D. 2008 Head-on collision of shock wave induced vortices with solid and perforated walls. *Phys. Fluids* **20** (1), 016104.

LI, X., HE, F., ZHANG, X., HAO, P., WU, X. & LIU, N. 2024 Experimental study on acoustic resonance of subsonic and slightly underexpanded impinging jets. *J. Fluid Mech.* **983**, A32.

LIU, N.-H., LI, X.-R., HAO, P.-F., ZHANG, X.-W. & HE, F. 2021 Mode switch in tonal under-expanded impinging jets. *Phys. Fluids* **33** (12), 124102.

MANNING, T. & LELE, S. 2000 A numerical investigation of sound generation in supersonic jet screech. In *21st AIAA Aeroacoustics Conference*. AIAA Paper AIAA-2000-2081.

MARCHIANO, R., COULOUVRAT, F., BASKAR, S. & THOMAS, J.-L. 2007 Experimental evidence of deviation from mirror reflection for acoustical shock waves. *Phys. Rev. E* **76** (5), 056602.

MARSH, A.H. 1961 Noise measurements around a subsonic air jet impinging on a plane, rigid surface. *J. Acoust. Soc. Am.* **33** (8), 1065–1066.

MASON-SMITH, N., EDGINGTON-MITCHELL, D., BUCHMANN, N.A., HONNERY, D.R. & SORIA, J. 2015 Shock structures and instabilities formed in an underexpanded jet impinging on to cylindrical sections. *Shock Waves* **25** (6), 611–622.

MCLAUGHLIN, D.K., MORRISON, G.L. & TROUTT, T.R. 1977 Reynolds number dependence in supersonic jet noise. *AIAA J.* **15** (4), 526–532.

MELLING, A. 1997 Tracer particles and seeding for particle image velocimetry. *Meas. Sci. Technol.* **8** (12), 1406–1416.

MINOTA, T., NISHIDA, M. & LEE, M.G. 1997 Shock formation by compressible vortex ring impinging on a wall. *Fluid Dyn. Res.* **21** (3), 139–157.

MINOTA, T., NISHIDA, M. & LEE, M.G. 1998 Head-on collision of two compressible vortex rings. *Fluid Dyn. Res.* **22** (1), 43–60.

MITCHELL, D.M., HONNERY, D.R. & SORIA, J. 2012 The visualization of the acoustic feedback loop in impinging underexpanded supersonic jet flows using ultra-high frame rate schlieren. *J. Vis. Japan* **15** (4), 333–341.

NAKASHIMA, Y. & INOUE, O. 2008 Sound generation by a vortex ring collision with a wall. *Phys. Fluids* **20** (12), 126104.

NOGUEIRA, P.A.S., JORDAN, P., JAUNET, V., CAVALIERI, A.V.G., TOWNE, A. & EDGINGTON-MITCHELL, D. 2022 Absolute instability in shock-containing jets. *J. Fluid Mech.* **930**, A10.

NOGUEIRA, P.A.S., CAVALIERI, A.V.G., MARTINI, E., TOWNE, A., JORDAN, P. & EDGINGTON-MITCHELL, D. 2024 Guided jet waves. *J. Fluid Mech.* **999**, A47.

NOSSEIR, N.S. & HO, C.-M. 1982 Dynamics of an impinging jet. Part 2. The noise generation. *J. Fluid Mech.* **116**, 379–391.

OZAWA, Y., NONOMURA, T., OYAMA, A. & ASAI, K. 2020 Effect of the Reynolds number on the aeroacoustic fields of a transitional supersonic jet. *Phys. Fluids* **32** (4), 046108.

PINEAU, P. & BOGEY, C. 2019 Steepened Mach waves near supersonic jets: study of azimuthal structure and generation process using conditional averages. *J. Fluid Mech.* **880**, 594–619.

POWELL, A. 1953 The noise of choked jets. *J. Acoust. Soc. Am.* **25** (3), 385–389.

POWELL, A. 1988 The sound-producing oscillations of round underexpanded jets impinging on normal plates. *J. Acoust. Soc. Am.* **83** (2), 515–533.

REICHMAN, B.O., GEE, K.L., NEILSEN, T.B., HALES SWIFT, S., WALL, A.T., MICAH DOWNING, J. & JAMES, M.M. 2022 Acoustic shock formation in noise propagation during military aircraft ground run-up operations. *AIAA J.* **60** (7), 4081–4090.

SAMIMY, M., KATTERLE, K., LEAHY, R., WEBB, N., YARLAGADDA, A. & HILER, N. 2024 Active control of flow and near-field pressure fluctuations in heated supersonic rectangular twin jets. *J. Fluid Mech.* **984**, A36.

SAMIMY, M., WEBB, N., ESFAHANI, A. & LEAHY, R. 2023 Perturbation-based active flow control in overexpanded to underexpanded supersonic rectangular twin jets. *J. Fluid Mech.* **959**, A13.

SHARIFF, K. & MANNING, T.A. 2013 A ray tracing study of shock leakage in a model supersonic jet. *Phys. Fluids* **25** (7), 076103.

SINIBALDI, G., LACAGNINA, G., MARINO, L. & ROMANO, G.P. 2013 Aeroacoustics and aerodynamics of impinging supersonic jets: analysis of the screech tones. *Phys. Fluids* **25** (8), 086104.

SUZUKI, T. & LELE, S.K. 2003 Shock leakage through an unsteady vortex-laden mixing layer: application to jet screech. *J. Fluid Mech.* **490**, 139–167.

TAM, C.K.W. & AHUJA, K.K. 1990 Theoretical model of discrete tone generation by impinging jets. *J. Fluid Mech.* **214**, 67–87.

TAM, C.K.W. & HU, F.Q. 1989 On the three families of instability waves of high-speed jets. *J. Fluid Mech.* **201**, 447–483.

TAM, C.K.W. & NORUM, T.D. 1992 Impingement tones of large aspect ratio supersonic rectangular jets. *AIAA J.* **30** (2), 304–311.

Towne, A., Cavalieri, A.V.G., Jordan, P., Colonius, T., Schmidt, O., Jaunet, V. & Brès, G.A. 2017 Acoustic resonance in the potential core of subsonic jets. *J. Fluid Mech.* **825**, 1113–1152.

Varé, M. & Bogey, C. 2022*a* Generation of acoustic tones in round jets at a Mach number of 0.9 impinging on a plate with and without a hole. *J. Fluid Mech.* **936**, A16.

Varé, M. & Bogey, C. 2022*b* Presence and properties of acoustic peaks near the nozzle of impinging rocket jets. *Acta Acust.* **6**, 36.

Varé, M. & Bogey, C. 2023 Mach number dependence of tone generation by impinging round jets. *AIAA J.* **61** (8), 1–15.

Webb, N., Esfahani, A., Yoder, S., Leahy, R. & Samimy, M. 2023 Empirical closure model for coupling mode prediction in supersonic rectangular twin jets. *AIAA J.* **61** (3), 1238–1247.

Weightman, J.L., Amili, O., Honnery, D., Edgington-Mitchell, D. & Soria, J. 2019 Nozzle external geometry as a boundary condition for the azimuthal mode selection in an impinging underexpanded jet. *J. Fluid Mech.* **862**, 421–448.

Weightman, J.L., Amili, O., Honnery, D., Edgington-Mitchell, D.M. & Soria, J. 2016 Supersonic jet impingement on a cylindrical surface. In *22nd AIAA/CEAS Aeroacoustics Conference*, AIAA Paper AIAA 2016-2800, p. 2800.

Weightman, J.L., Amili, O., Honnery, D., Edgington-Mitchell, D.M. & Soria, J. 2017*a* On the effects of nozzle lip thickness on the azimuthal mode selection of a supersonic impinging flow. In *23rd AIAA/CEAS Aeroacoustics Conference*, AIAA Paper AIAA 2017-3031, p. 3031.

Weightman, J.L., Amili, O., Honnery, D., Soria, J. & Edgington-Mitchell, D. 2017*b* An explanation for the phase lag in supersonic jet impingement. *J. Fluid Mech.* **815**, R1.

Willert, C.E., Mitchell, D.M. & Soria, J. 2012 An assessment of high-power light-emitting diodes for high frame rate schlieren imaging. *Exp. Fluids* **53** (2), 413–421.

Willis, W.A.III, Cormack, J.M., Tinney, C.E. & Hamilton, M.F. 2023 Reduced-order comparison of simulated and measured coalescing Mach waves near supersonic jets. *AIAA J.* **61** (5), 2022–2034.

Young, S.M., Gee, K.L., Neilsen, T.B. & Leete, K.M. 2015 Outdoor measurements of spherical acoustic shock decay. *J. Acoust. Soc. Am.* **138** (3), EL305–EL310.